ACS APPLIED MATERIALS & INTERFACES

Research Article

www.acsami.org

Interface Effect on the Electropolymerized Polypyrrole Films with Hollow Micro/Nanohorn Arrays

Yang Bai, Youlong Xu,* Jie Wang, Mingqi Gao, and Jingping Wang

Electronic Materials Research Laboratory, Key Laboratory of the Ministry of Education & International Center of Dielectric Research, Xi'an Jiaotong University, Xi'an 710049, Shaanxi, P.R. China

Supporting Information

ABSTRACT: Polypyrrole (PPy) films with hollow micro/nanohorn arrays were controllably synthesized in p-toluenesulfonate aqueous solutions by template-free electrochemical methods. The micelles which consist of pyrrole monomers and the surfactants provided the soft templates during the polymerization process. The polymerization potential and pH value of the solutions cooperatively influenced the shape of the micelles at the substrate/electrolyte interface and further controlled the morphologies of PPy films. PPy grew along the soft templates during the high potential periods of a pulse potentiostatic (PPS) method, while the pH value and the low potential were varied to modulate the shape of the soft templates. It has been shown to be most appropriate to fabricate hollow micro/nanohorn PPy films with the highest electrical conductivity (190 S cm^{-1}) via PPS at pH ~1.5. A diagram was also introduced in order to illustrate the polymerization potential and pH value dependence of nanohorn PPy morphologies. This work proposed a potential method to the in situ growth of conducting polymers with high conductivity and high specific surface area.

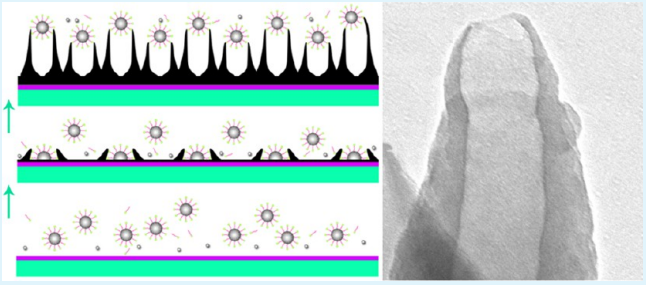

KEYWORDS: *conducting polymer, template-free, soft template, pulse potentiostatic method, surfactant, specific surface area*

INTRODUCTION

Polypyrrole (PPy) is one of the most widely studied conducting polymers due to its advantages in high conductivity, low material cost, ease of synthesis, and environmentally friendly features.[1,2] In recent years, PPy has been widely applied as the functional materials in energy storage,[3−5] drug delivery,[6,7] chemical or biological sensors,[8,9] actuators,[10] artificial muscles,[11] corrosion inhibitors,[12] solar cells,[13,14] etc.

Numerous conducting polymer micro/nanostructures have been synthesized to obtain superior physical and chemical properties compared to their bulky counterparts. The micro/nanostructured PPy is generally synthesized by chemical or electrochemical methods. The electrochemical method has several advantages in comparison with the chemical method. First, the films can be in situ prepared on substrates, leading to high adhesion strength. Second, the thickness and mass of films are easy to be controlled during the electrochemical polymerization process.[1,15,16] At last, the different morphology and electrically conducting properties of films are obtained by different electrochemical methods. A lot of work has shown that electrochemical polymerization is a one-step and effective technique for preparing micro/nanostructured PPy with controlled morphologies and properties.[17−20]

Micro/nanostructured PPy are commonly prepared via a hard template method with the use of hard porous membranes as the hard templates.[21−24] The morphologies of the PPy are easy to control with the help of the hard templates, but the high cost and complex preparation process usually limited the application of hard template methods. In addition, the micro/nanostructures may be damaged during the removal process of the hard template method. Hence, more attention has been paid on template-free (also called soft template or molecule template) methods for the preparation of micro/nanostructured PPy.[25−27] The template-free method is usually realized by self-assembly of surfactant ions in the solution which do not need to be removed after the polymerization.

Several successful special examples are reported for growing oriented micro/nanostructured PPy through the template-free electrochemical technique. PPy microcontainers have been electrochemically generated with gas bubbles working as the templates in early works.[28−30] Recently, PPy nanowires have also been electrochemically synthesized using perchlorate (ClO_4^-) based chemical additives.[31,32] In our previous work, PPy with micro/nanohorn structure was galvanostatically prepared in a basic aqueous solution and has shown good properties in supercapacitors.[33] However, a simple and controllable template-free electrochemical technique has not been developed for growing oriented micro/nanostructured PPy. Moreover, it is obvious that the growth mechanism remains to perfect further.

Received: November 12, 2013
Accepted: March 10, 2014
Published: March 10, 2014

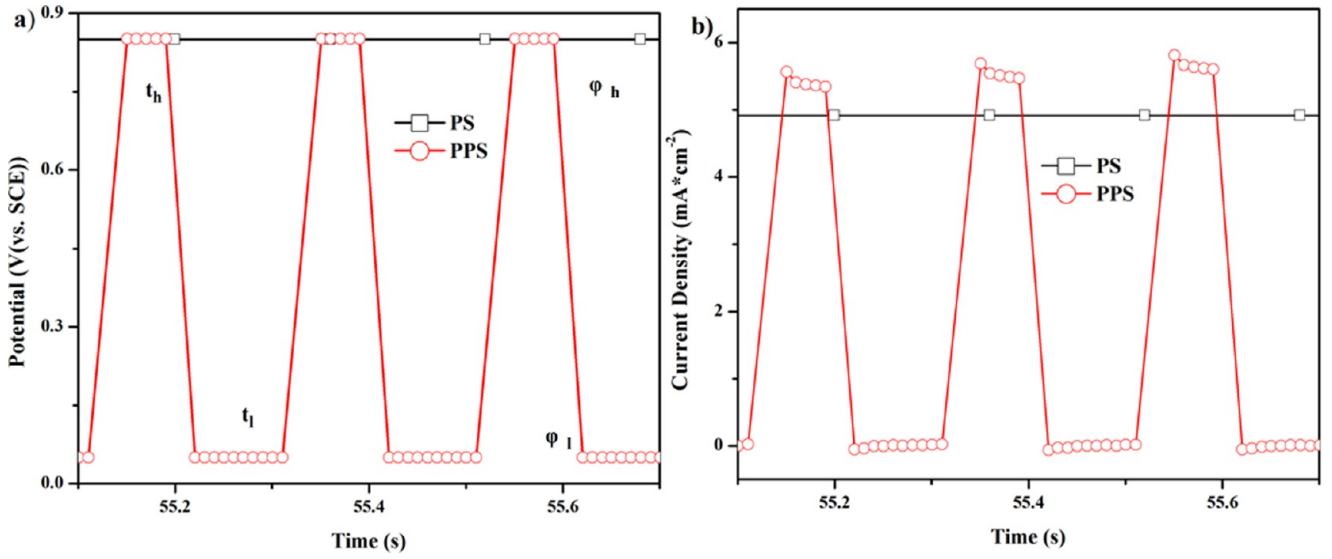

Figure 1. Schematics of the potentiostatic method (PS) and pulse potentiostatic method (PPS) (a) and the corresponding current density (b).

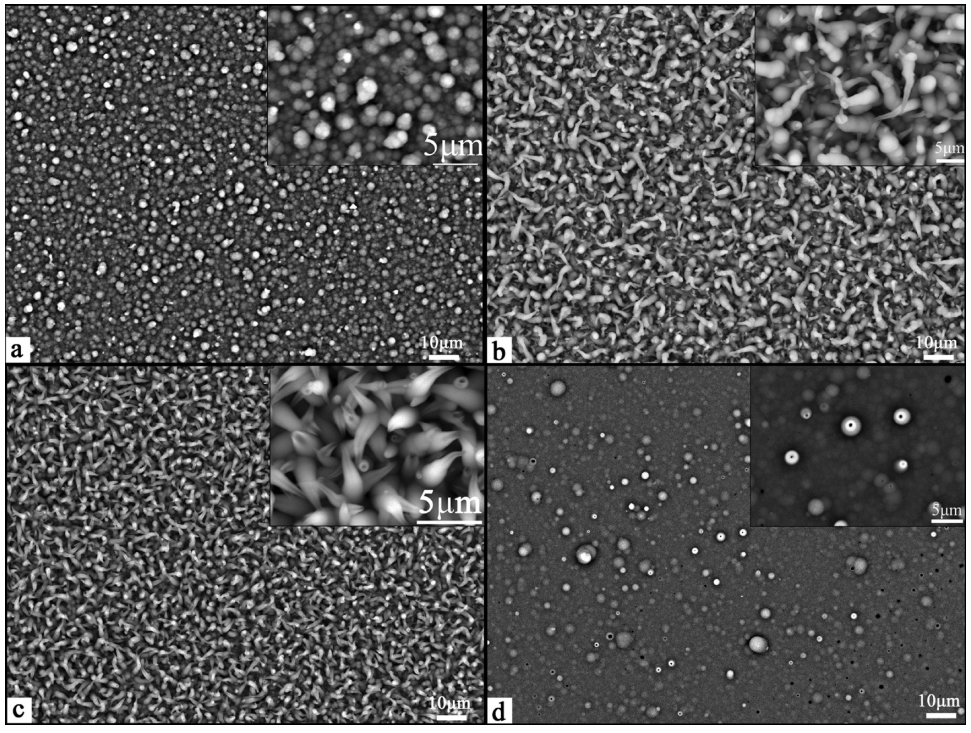

Figure 2. SEM images of the top view of the typical PPy@A-PS (a), PPy@B-PS (b), PPy@A-PPS (c), and PPy@B-PPS (d).

In this work, the micelles which consist of pyrrole monomers and the surfactants provided the soft templates for the synthesis of micro/nanohorn arrays. We adopt a modified pulse potentiostatic method (PPS) to modulate the shape of the micelles at the substrate/electrolyte interface and further control the morphologies of PPy films. Variation of the low potential of PPS was applied for the first time in order to control the morphologies. The influence of other electrochemical polymerization conditions, such as pH value of the polymerization solution, polymerization charge, and concentration of TOS^-, on the morphologies was also investigated. A diagram was introduced for an overview of the favorable region for the growth of hollow micro/nanohorns arrays. The detailed mechanism on oriented micro/nanostructured PPy growing at different conditions was presented and explained. PPS has been shown to be a facile approach to fabricate hollow micro/nanohorn PPy films with improved electrical conductivity properties.

EXPERIMENTAL SECTION

Synthesis of PPy Films. Pyrrole monomer (Py, Capchem, 99%) was twice distilled prior to use. p-Toluenesulfonic acid (TOSH, China Medicine Group, AR) and the sodium p-toluenesulfonic (TOSNa, China Medicine Group, CP) were used as received. The acid aqueous solution contained 300 mM pyrrole, 100 mM TOSH, and 400 mM TOSNa with pH = 1.5, while the basic one contained 300 mM pyrrole and 500 mM TOS^-, and the pH value was adjusted with sodium hydroxide (NaOH, China Medicine Group, CP) to 9.5. The pH value of the basic solution was monitored by an advanced pH value meter

dx.doi.org/10.1021/am500513u | ACS Appl. Mater. Interfaces 2014, 6, 4693−4704

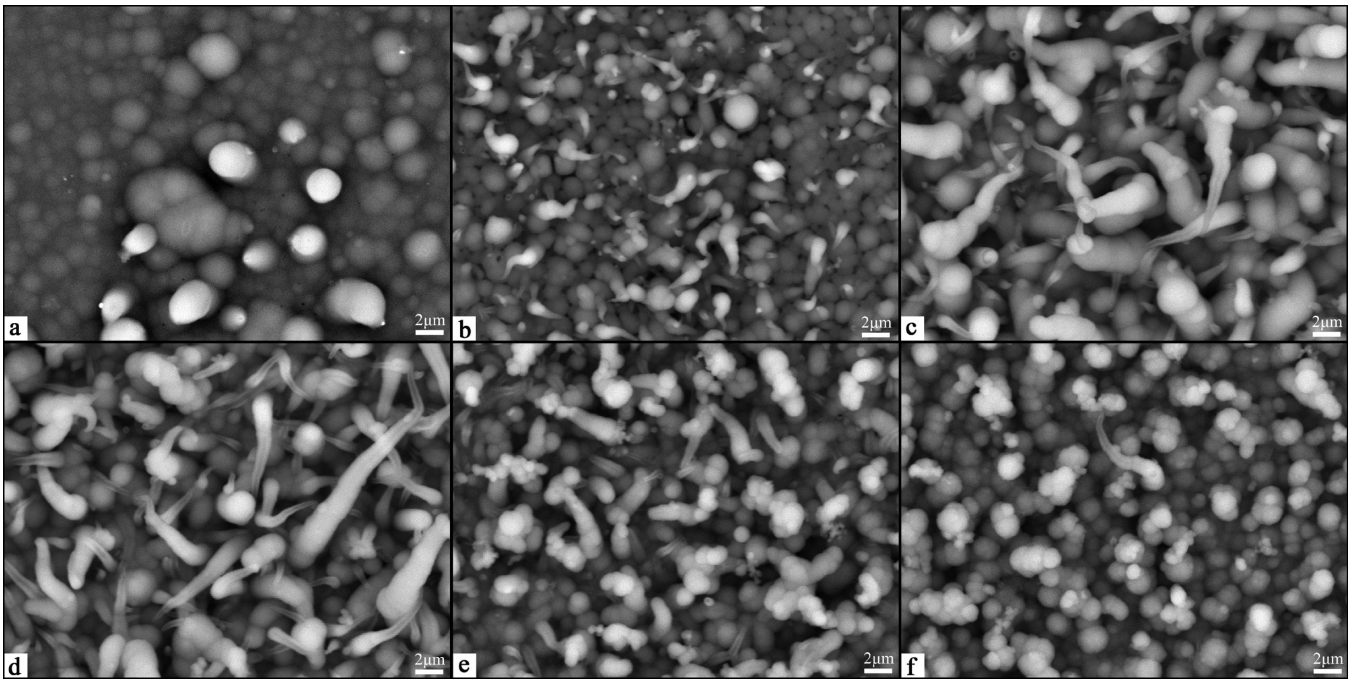

Figure 3. SEM images of the top view of PPy@B-PS. The applied potential is 750 mV (a), 850 mV (b), 1200 mV (c), 1500 mV (d), 2100 mV (e), and 3000 mV (f), respectively.

and kept constant by adding TOSH solution frequently during the polymerization. The reason for the change of the pH value has been discussed in our previous work[33] and in the Supporting Information (SI). The electrodeposition was carried out in a three-electrode cell. The tantalum sheet was used as counter electrode, and the electrochemical potentials were measured against a saturated calomel electrode (SCE). All FTO glasses (Nippon Sheet Glass, 14Ω·sq^{-1}) were chosen as the working electrode (considering the potential application of PPy in dye-sensitized solar cells as counter electrodes). All polymerizations were performed in an ice−water bath.

A Versatile Multichannel Potentiostat 2/Z (VMP2, Princeton Application Research) was used to perform all the electrochemical preparation of the PPy films. The PPy films were prepared under either potentiostatic (PS) or pulse potentiostatic (PPS) conditions in both acid (A) and basic (B) solutions, and they will be referred to as PPy@A-PS, PPy@B-PS, PPy@A-PPS, and PPy@B-PPS, respectively. The schematic plot of PS and PPS is illustrated in Figure 1a. φ_h and φ_l are the high and low potentials of PPS, respectively; t_h and t_l are the corresponding periods. Figure 1b shows the corresponding current density. In this study, the PPy films were prepared with the equivalent total polymerization charge of 500 mC*cm^{-2}, unless when the polymerization charge was discussed and when the PPy films were used for the measurement of FTIR and conductivity. The formed PPy films were washed with deionized water and dried at 55 °C in the atmosphere.

Characterization and Measurement. The morphologies of the as-prepared PPy films were observed by a scanning electron microscopy (SEM, Hitachi, Model S-4800) and a transmission electronic microscope (TEM, JEOL, JEM-2100). The resonance Raman spectroscopy was obtained by LabRAM HR800 Raman microscope (Horiba Jobin Yvon). The PPy films for the Fourier transform infrared spectroscopy (FTIR) and conductivity measurement were polymerized with a polymerization charge of 1.5 C*cm^{-2} and peeled off from FTO. The chemical nature of PPy films was ascertained using FTIR (Bruker, VERTEX 70) by the attenuated total reflection (ATR) mode. The room temperature electronic conductivity was tested with the four-probe method (Guangzhou 4 probes Tech, RTS-9) after being pressed under the pressure of 15 MPa. The presence of micelles filled with pyrrole monomers was verified with Zetasizer Nano instrument (Malvern, ZEN3690).

RESULTS AND DISCUSSION

1. Morphologies of PPy Synthesized in Different Conditions. Figure 2 shows the typical morphologies of PPy@A-PS, PPy@B-PS, PPy@A-PPS, and PPy@B-PPS. When the potentiostatic method is applied (850 mV/SCE), the conventional typical cauliflower-like PPy films would be synthesized in acid solutions, shown in Figure 2a, referred to as PPy@A-PS. The film thus obtained comprises a layer of compact PPy film at the bottom and a cauliflower-like PPy film with a diameter of 1−2 μm on top of it. In the case of basic solutions and the potentiostatic method (1200 mV/SCE), the surface morphology of the obtained PPy film is shown in Figure 2b, referred to as PPy@B-PS. There are micro/nanohorns growing on the surface though the horns are not so dense or homogeneous, and they show an average diameter of approximately 100 nm at the free end, 1−10 μm in length. The density of micro/nanohorns is about 10^6−10^7 per cm^2 according to the SEM image (Figure 2b). As shown in Figure 2c, when PPS is applied in acid solutions, dense and homogeneous hollow micro/nanohorn arrays would come out on the substrate, mentioned as PPy@A-PPS. The PPy micro/nanohorns are almost perpendicularly aligned on the substrate surface to form arrays. They show an average diameter of approximate 100 nm at the free end, 2 μm at the bottom, and ∼5 μm in length. There are about 10^7−10^8 micro/nanohorns per cm^2 according to the SEM image. On the other hand, when PPS is applied in basic solutions (PPy@B-PPS), only a few short micro/nanohorns are left, as shown in Figure 2d. Discussion of the details of PPy@A-PS, PPy@B-PS, PPy@A-PPS, and PPy@B-PPS will be taken up in the following parts. The effects of polymerization charge and TOS^- concentration on the morphologies are also discussed to investigate the formation of the micro/nanohorn arrays.

1.1. Morphologies of PPy@A-PS. The morphologies of PPy@A-PS are cauliflower-like when the potential is below water electrolysis, as mentioned in previous works,[34] shown in Figure 2a. The size of cauliflowers changes little with the

dx.doi.org/10.1021/am500513u | ACS Appl. Mater. Interfaces 2014, 6, 4693−4704

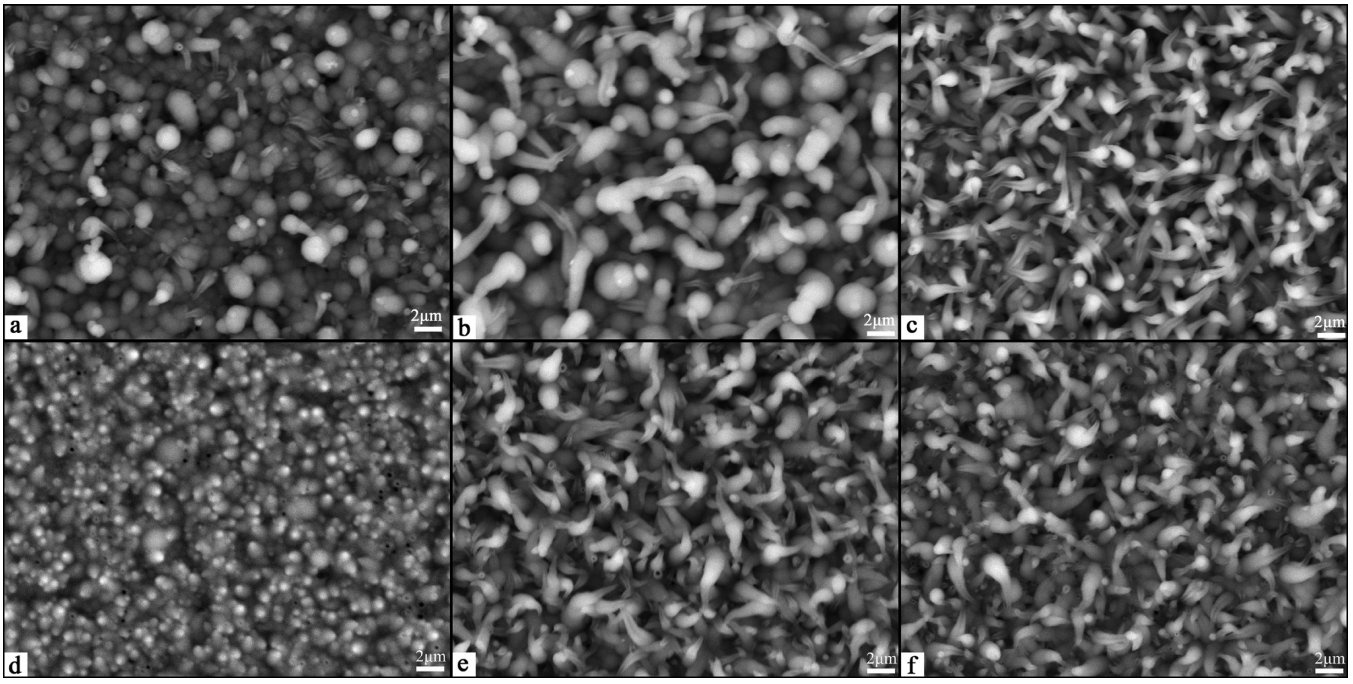

Figure 4. SEM images of the PPy@A-PPS films prepared with different φ_l and t_l. φ_l = 550 mV, t_l = 160 ms (a), φ_l = 350 mV, t_l = 160 ms (b), φ_l = −50 mV, t_l =160 ms (c), φ_l = −450 mV, t_l = 160 ms (d), φ_l = −50 mV, t_l =100 ms (e), φ_l = −50 mV, t_l =40 ms (f).

applied potential. When the applied potential is higher than 2100 mV/SCE, there are some microcontainers formed as discussed by other authors,[29,28] as is shown in Figure S1. Briefly, the microcontainers are formed by O_2 released from the electrolysis of water in aqueous solutions. The morphologies of micro/nanohorn arrays discussed here are quite different from the microcontainers. So we presume here that the formation of micro/nanohorns bears no relationship with the gas bubbles and do not take it into account in this paper.

1.2. Morphologies of PPy@B-PS. Figure 3 shows the morphologies of PPy@B-PS polymerized with different potentials. When the applied potential is as low as 750 mV/SCE (Figure 3a), the morphologies are similar to cauliflower-like, and some of the cauliflowers grow higher. When the potential is set to 850 mV/SCE (Figure 3b), some micro/nanohorns begin to appear, and the length is about 2−4 μm. As the potential further increases, more micro/nanohorns grow up, and the length increases with the increase of the applied potential (Figure 3c, d). The longest micro/nanohorn is over 20 μm when the potential is 1500 mV/SCE. When the applied potential is high up to 2100 mV/SCE (Figure 3e), the density and the length of the micro/nanohorns decreases, and when it further increases to 3000 mV/SCE (Figure 3f), micro/nanohorns could hardly be seen and turn back to cauliflower-like. The result of PPy@B-PS is similar to PPy galvanostatically prepared in a basic aqueous solution in our previous work.[33]

1.3. Morphologies of PPy@A-PPS. Four tunable parameters are concerned in the pulse potentiostatic method (PPS): the high potential (φ_h), the period time of the high potential (t_h), the low potential (φ_l), and the period time of the low potential (t_l). The effect of these four parameters on the morphologies of PPy@A-PPS will be systematically investigated.

1.3.1. Effect of φ_l and t_l on Morphologies of PPy@A-PPS. The surface morphologies of PPy@A-PPS polymerized with different φ_l and t_l are shown in Figure 4. For samples in Figure 4a−d, φ_l is 550 mV/SCE (Figure 4a), 350 mV/SCE (Figure 4b), −50 mV/SCE (Figure 4c), and −450 mV/SCE (Figure 4d), respectively, under otherwise identical conditions (φ_h: 850 mV/SCE, t_h: 100 ms, t_l: 160 ms). When φ_l is set to be 550 mV/SCE (Figure 4a), scattered micro/nanohorns can be found dispersing between the cauliflowers regardless of the length. It can be assumed to be the transition state from the cauliflower-like structure to horn-like structure. As φ_l decreases to 350 mV/SCE (Figure 4b), horns grow longer and more. When −50 mV/SCE is applied (Figure 4c), dense and uniform micro/nanohorn arrays would be obtained. Interestingly, further decreasing φ_l to −450 mV/SCE causes the micro/nanohorns to diminish, rendering micro/nanohorns thus obtained much shorter and smaller. It appears that the growth of the horns stops very quickly after the beginning. The morphology of the PPy films is strongly influenced by φ_l, and approximately −50 mV/SCE is optimum to form the dense and homogeneous horn-like structures. Thus, −50 mV/SCE is selected as the optimum φ_l for subsequent studies. The influence of t_l on the morphologies will be discussed next. For samples in Figure 4c,e,f, t_l is set as 160 ms, 100, and 40 ms, respectively, while the other parameters are kept constant (φ_h: 850 mV/SCE, φ_l: −50 mV/SCE, t_h: 100 ms). The sample of PPy@A-PS (Figure 2a) is considered as the one prepared with t_l of 0 ms. With the decrease of t_l from 160 ms to 0 ms, the morphologies of the films graduate from horn-like to cauliflower-like structures. For short t_l, for instance, 40 ms (Figure 4f), micro/nanohorns and cauliflowers are mixed on the surface and the micro/nanohorns are less uniform. t_l longer than 160 ms increases only the polymerization time and has no positive effects on formation of micro/nanohorns (not shown). As discussed above, φ_l and t_l are the crucial factors in the formation of micro/nanohorn arrays. The formation of such a structure requires φ_l of about −50 mV/SCE and a relatively long t_l.

1.3.2. Effect of φ_h and t_h on Morphologies of PPy@A-PPS. The effects of the high potential period (φ_h and t_h) on the morphologies of PPy@A-PPS samples are investigated, and the

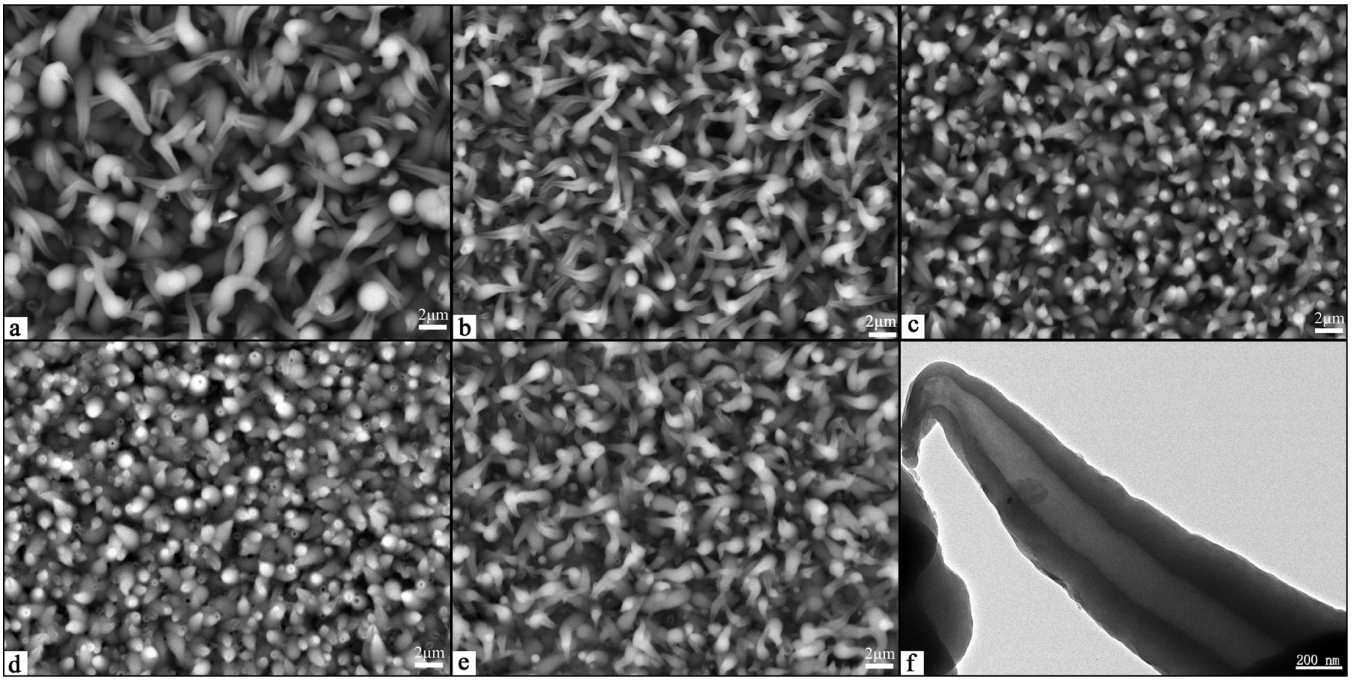

Figure 5. SEM images of the PPy@A-PPS films prepared with different φ_h and t_h. φ_h = 950 mV, t_h = 100 ms (a), φ_h = 850 mV, t_h = 100 ms (b), φ_h = 750 mV, t_h = 100 ms (c), φ_h = 850 mV, t_h = 40 ms (d), φ_h = 850 mV, t_h = 160 ms (e). TEM image of one micro/nanohorn (f).

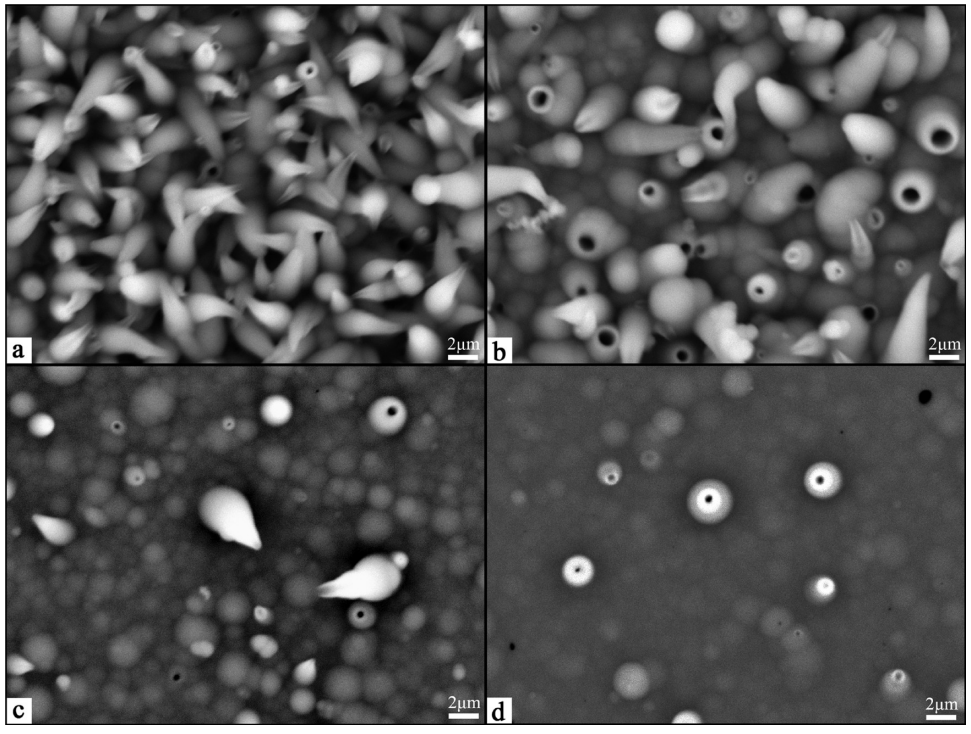

Figure 6. SEM images of the PPy@B-PPS films prepared with different t_l, 40 ms (a), 60 ms (b), 80 ms (c), and 120 ms (d), respectively.

corresponding surface morphologies of the PPy films are shown in Figure 5. At first, we apply different φ_h (950 mV/SCE, 850 mV/SCE, and 750 mV/SCE) and keep φ_l, t_h, and t_l constant (−50 mV/SCE, 100 and 160 ms, respectively). When the potential is relatively high (950 mV/SCE, Figure 5a), the micro/nanohorns are longer but sparser. We can also see that some of the micro/nanohorns turn closed-ended or even cauliflower-like. In contrast, when the potential is relatively low (750 mV/SCE, Figure 5c), there are more micro/nanohorns formed but with a short length, and most of the micro/nanohorns keep their ends open. Then we discuss the effects of t_h. The morphologies of PPy films polymerized with a short t_h (40 ms, Figure 5d) are similar to that with a relatively low φ_h (Figure 5c). Dense, short, and open-ended micro/nanohorns distribute uniformly on the surface of PPy films. When a relatively long t_h (160 ms, Figure 5e) is adopted, the micro/nanohorns are longer but sparser, and some of them turn closed-ended, which is similar to Figure 4b, Figure 4f, and

dx.doi.org/10.1021/am500513u | ACS Appl. Mater. Interfaces 2014, 6, 4693−4704

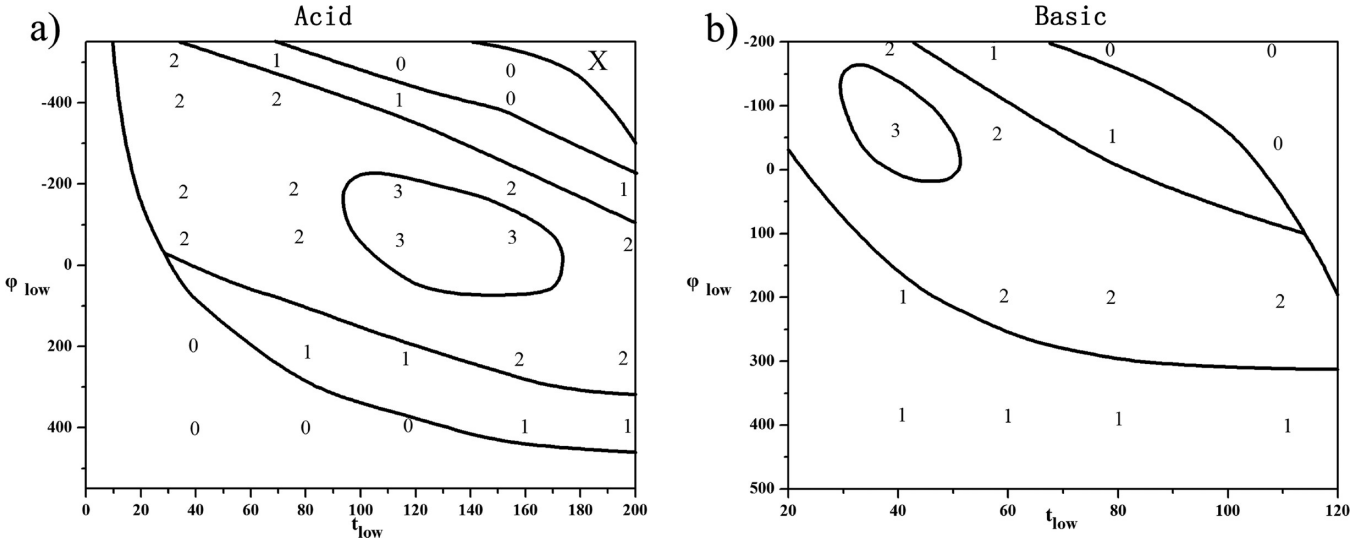

Figure 7. Diagrams for the PPy micro/nanohorn arrays polymerized in acid (a) and basic solutions (b).

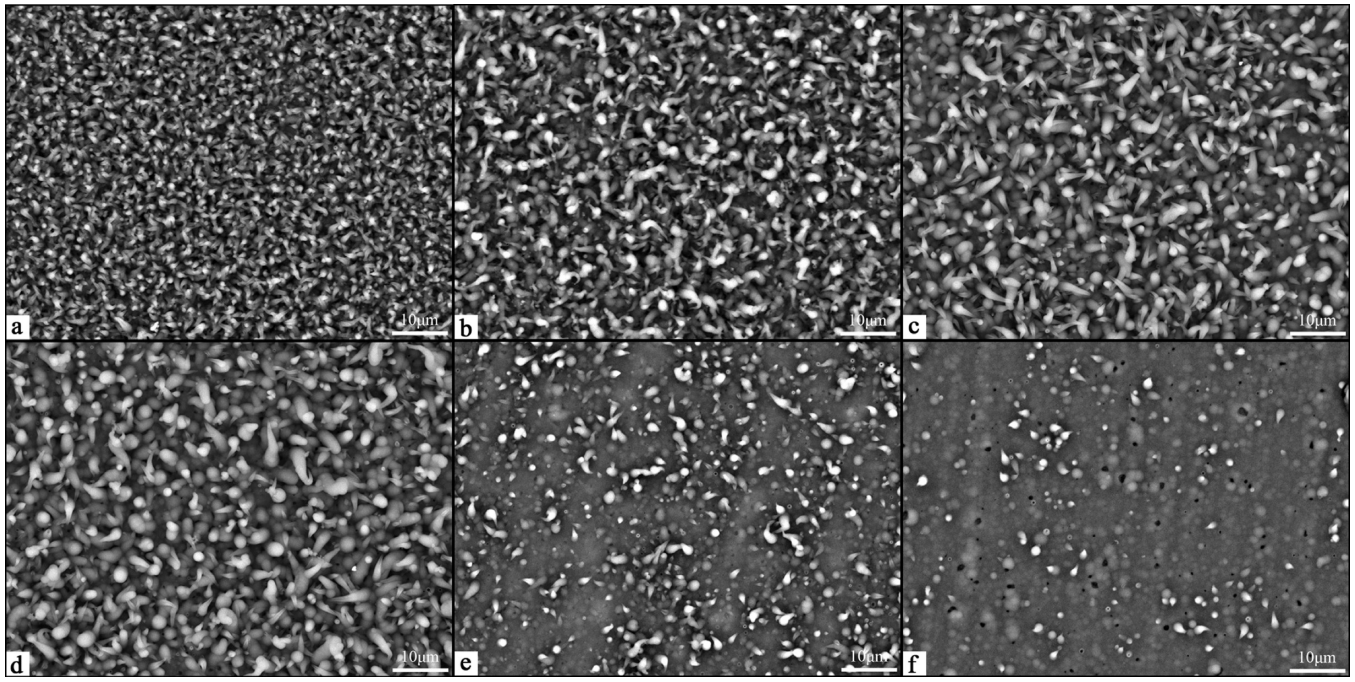

Figure 8. SEM images of the PPy@A-PPS films prepared with different TOS^- concentration, 500 mM (a), 200 mM (b), 100 mM (c), 50 mM (d), 20 mM (e), and 10 mM (f), respectively.

Figure 5a. When φ_h is even higher (Figure 5a), t_h is too long (Figure 5e), φ_l is not low enough (Figure 4b), or t_l is not long enough (Figure 4f), the micro/nanohorns turn into closed-ended or even cauliflower-like. Figure 5f is the TEM image of one micro/nanohorn. The micro/nanohorn is hollow with a more or less constant internal pore diameter except the end. PPy turns thinner from the bottom to the tail end.

1.4. Morphologies of PPy@B-PPS. The surface morphologies of PPy@B-PPS with different t_l are shown in Figure 6. T_l is 40 ms (Figure 6a), 60 ms (Figure 6b), 80 ms (Figure 6c), and 120 ms (Figure 6d), respectively, while the other three parameters are kept constant (φ_h: 1200 mV/SCE, t_h: 100 ms, φ_l: −50 mV/SCE). We can see that a relatively short t_l is helpful to get dense and uniform micro/nanohorn arrays by comparing Figure 6a (PPy@B-PPS) and Figure 3c (PPy@B-PS). Surprisingly that when t_l increases to 60 ms, there are fewer micro/nanohorns, and most of them are open-ended (Figure 6b). If t_l further increases to 80 ms, most of the surface is flat, and quite a few micro/nanohorns turn up (Figure 6c). When 120 ms is applied, the film turns flatter, and the micro/nanohorns are very short (Figure 6d). It seems that with long t_l nanohorns cease to grow.

1.5. Diagrams for Polymerization Conditions of Micro/Nanohorn Structure. A diagram for the micro/nanohorn arrays is summarized and shown in Figure 7. The numbers marked in the regions roughly represent some level of uniformity of micro/nanohorns arrays wherein the bigger is the number, the more homogeneous and dense the micro/nanohorns arrays are. *X* represents no PPy polymerization and 0 means PPy films without micro/nanohorns. Each number corresponds to an

dx.doi.org/10.1021/am500513u | ACS Appl. Mater. Interfaces 2014, 6, 4693−4704

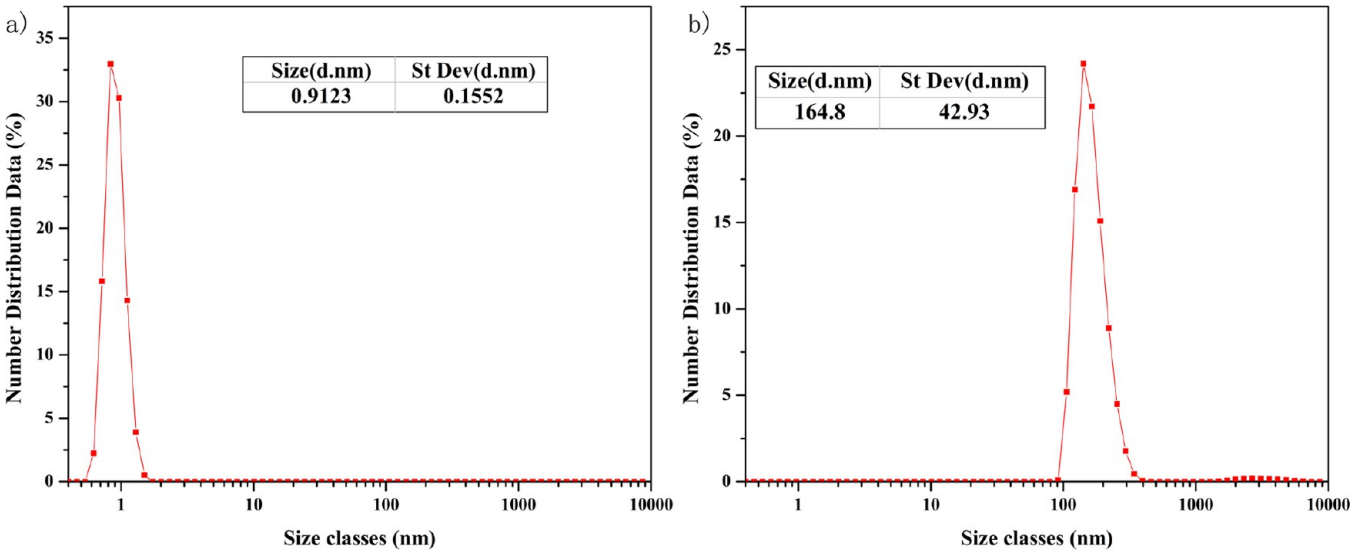

Figure 9. The number particle size distribution of the aqueous solution containing only 300 mM pyrrole (a) and the number particle size distribution of the aqueous solution containing 300 mM pyrrole, 100 mM TOSH, and 400 mM TOSNa (b).

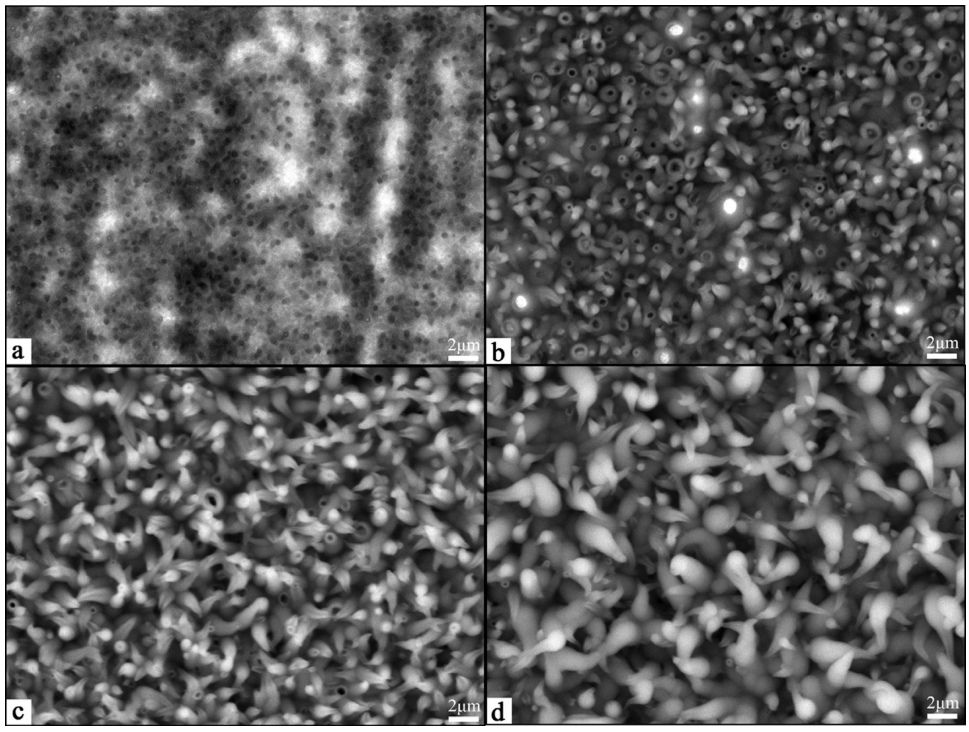

Figure 10. SEM images of the PPy films prepared with different polymerization charge, 100 mC (a), 200 mC (b), 400 mC (c), and 1000 mC (d), respectively.

SEM image which is given in this article and the SI. Samples shown in Figure 7a are prepared in acid solutions, and they are synthesized with the same φ_h (850 mV/SCE) and t_h (100 ms) and different φ_l, t_l. When φ_h or t_h increases, micro/nanohorns require lower φ_l and longer t_l. In contrast, when φ_h or t_h decreases, higher φ_l and lower t_l are required for the growth of micro/nanohorns; but when φ_h or t_h is too big or too small, only cauliflower-like PPy or none could be formed. Samples shown in Figure 7b are prepared in basic solutions, and similar things would happen when different φ_h and t_h are applied.

2. Discussion about the Polymerization Processes. *2.1. Effect of TOS^- Concentration on Morphologies.* The influence of the TOS^- concentration on the morphologies is shown in Figure 8, taking PPy@A-PPS as an example here. The molar ratio of TOSH and TOSNa is kept at 1:4, while the Py concentration (0.3 M) and the applied potential (φ_h 850 mV/SCE, φ_l −50 mV/SCE, t_h 100 ms, and t_l 160 ms) remain the same. The concentration of TOS^- is 500 mM, 200 mM, 100 mM, 50 mM, 20 mM, and 10 mM, respectively. The corresponding morphologies are shown in Figure 8. A lower amplification is applied to take the SEM images in order to provide a better view on the whole morphologies. When the concentration is higher than 500 mM, the morphologies are similar to Figure 8a, and it is not shown here. The micro/

dx.doi.org/10.1021/am500513u | ACS Appl. Mater. Interfaces 2014, 6, 4693−4704

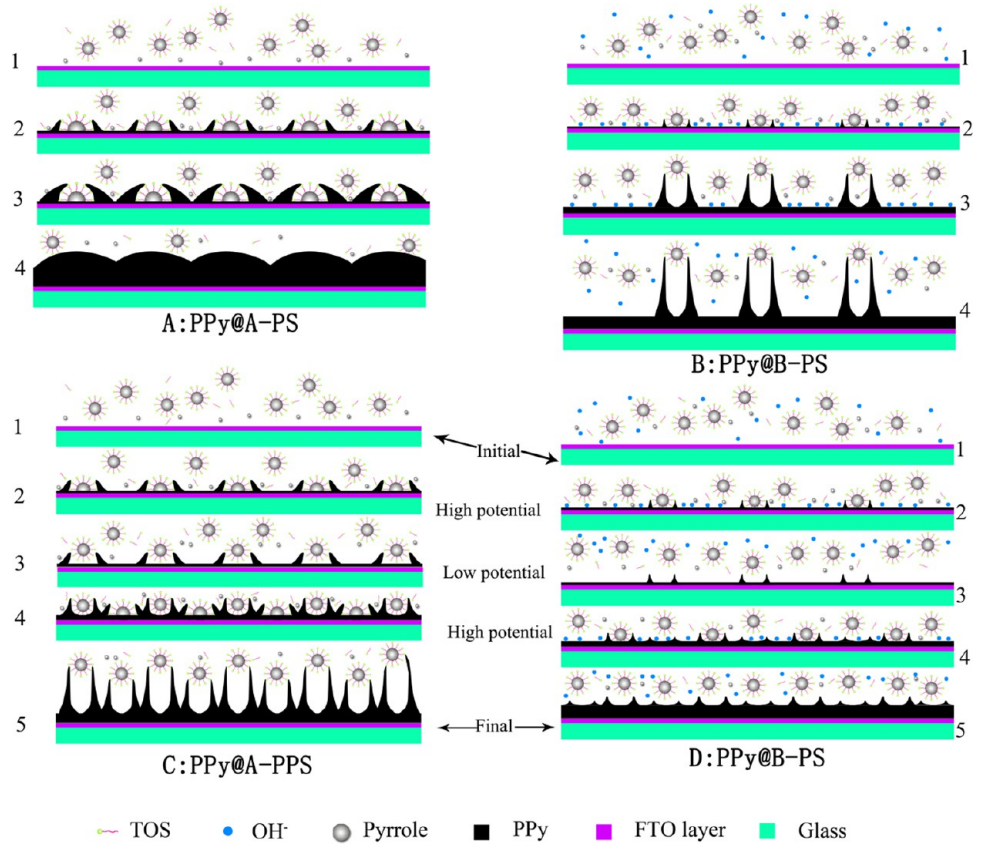

Figure 11. Schematics of the polymerization process of PPy@A-PS (A), PPy@B-PS (B), PPy@A-PPS (C), and PPy@B-PPS (D).

nanohorns turn sparser as the decrease of the TOS^- concentration. When the concentration is 10 mM, quite a few micro/nanohorns could be found. TOS^- can be thereby considered as a critical factor in the formation of micro/nanohorns.

It is commonly known that surfactants and pyrrole monomers spontaneously form micelles in aqueous solution because of the hydrophobic interactions between hydrocarbon chains of the surfactants and pyrrole monomers. The micelles could act as templates for synthesizing materials with various kinds of morphologies.[34,35] The presence of the micelles is verified with a Zetasizer Nano instrument. Figure 9a shows the number particle size distribution of the aqueous solution containing only 300 mM pyrrole monomers, and Figure 9b shows the number particle size distribution of the aqueous solution containing 300 mM pyrrole, 100 mM TOSH, and 400 mM TOSNa. We can see that there is no micelle in the solution when no TOS^- is dissolved in the solution. When TOS^- is added, the micelles show an average diameter of 164.8 nm with a standard deviation of 42.93 nm. The size of the micelles is consistent with the inner diameter of the micro/nanohorns (Figure 5f). In this study, we assume that micelles work as the soft templates for the micro/nanohorns.

2.2. Growing Process of Micro/Nanohorns. Morphologies for different polymerization charges (Q) are observed to investigate the growing process of the micro/nanohorns. Here we take PPy@A-PPS as examples. The samples are prepared with a charge of 100 mC, 200 mC, 400 mC, and 1000 mC, respectively, and the corresponding morphologies are shown in Figure 10. At the beginning of the polymerization (Figure 10a), black dots can be observed on the surface besides a thin film of PPy. When Q is 200 mC (Figure 10b), the growth of the micro/nanohorns is obvious. Most of the micro/nanohorns are short and open-ended. As the polymerization goes on (400 mC, Figure 10c), the micro/nanohorns grow longer. The micro/nanohorns continue growing until Q reaches 1000 mC, while some of the micro/nanohorns turn closed-ended and terminate their growth (Figure 10d). Simultaneously, new micro/nanohorns start their growth.

2.3. Probable Schematics of Polymerization Processes. According to the above discussion, the pH value, the applied potential, and the TOS^- concentration strongly affect the morphologies of PPy films. We assume that the micelles which consist of pyrrole monomers and the surfactants provided the soft templates during the polymerization process. The polymerization potential and pH value of the solutions cooperatively influenced the shape of the micelles at the substrate/electrolyte interface and further controlled the morphologies of PPy films. The micelles are covered with a monolayer of the surfactant on the surface and filled with pyrrole monomers in the middle.[36,37] In this study, TOS^- works as the surfactant as well as the dopant in the polymerization process. The hydrophobic groups of the surfactants are connected to pyrrole in the middle, and the hydrophilic groups are exposed to the water, as shown in Figure 11. The micelles are negative charged consequently. Based on the experimental results, we propose the growth mechanisms for the template-free electrochemical synthesis of PPy films with hollow micro/nanohorn arrays.

The difference of the polymerization environment between PPy@A-PS and PPy@B-PS in terms of the polymerization condition is the concentration of OH-, Figure 11A1, B1. For

dx.doi.org/10.1021/am500513u | ACS Appl. Mater. Interfaces 2014, 6, 4693−4704

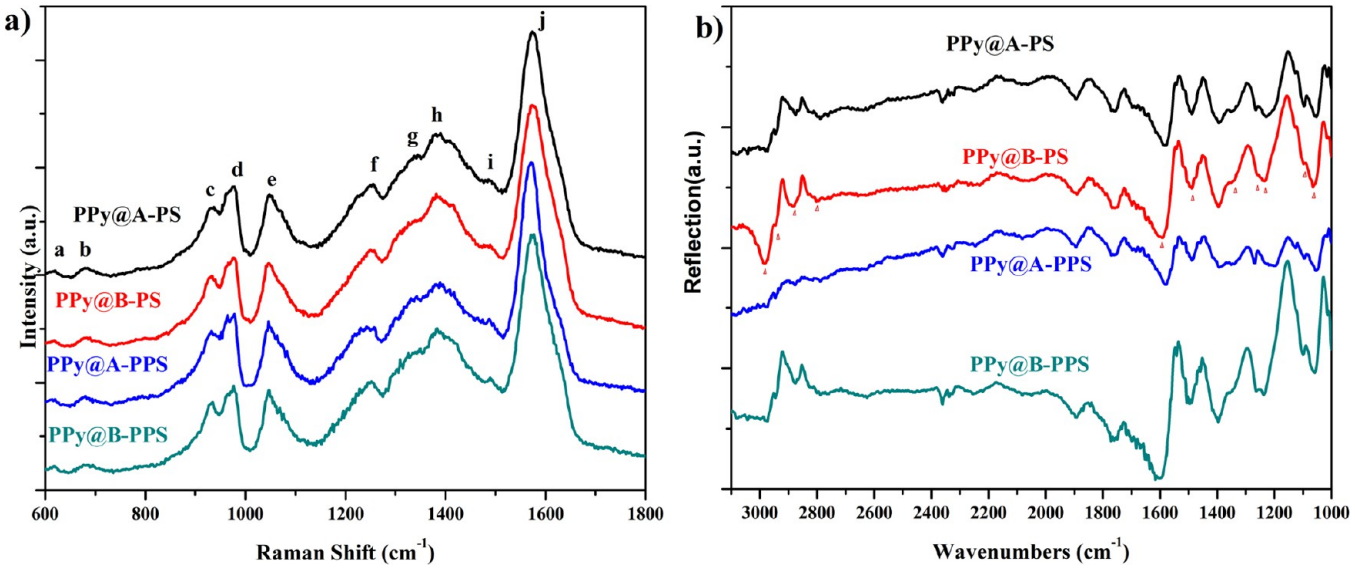

Figure 12. Raman spectra (a) and FTIR (b) of PPy@A-PS, PPy@B-PS, PPy@A-PPS, and PPy@B-PPS films.

PPy@B-PS, when the polymerization starts, OH^- moves faster toward the substrate than the micelles, and a layer of OH^- would be adsorbed on the surface of the substrate. The micelles and OH^- are both negatively charged, so the micelles for PPy@B-PS are farther from the substrate than those for PPy@A-PS. The shapes of the micelles which are absorbed at the substrate/electrolyte interface are different. The highest electric field is at the edge of the contact interface between the adsorbed micelles and the substrate because of the edge effect. Polypyrrole is predominately synthesized at the edge as a result, as shown in Figure 11A2, B2. For PPy@A-PS, the micelles could attach well to the substrate in the presence of the applied electric field. Polypyrrole grows along the micelles, and the cauliflower-like structure forms finally (Figure 11A3, A4). For PPy@B-PS, the contact area between the adsorbed micelles and the substrate is smaller, and polypyrrole growing along the micelles thereby may be aligned perpendicular to the substrate. The micelles are pushed higher by the polypyrrole which is unremittingly growing higher. Finally, the horn-like structure is thus formed, as shown in Figure 11B3, B4. The polymerization of pyrrole along the edge of the micelles would finally produce the hollow "horns". We gave a speculation on the polymerization process of PPy which were galvanostatically prepared in a basic aqueous solution in our previous work.[33] The result of PPy@B-PS and the existence of the micelles further verified that speculation and the schematic of polymerization process of PPy@B-PS given in this work is similar to that. For PPy@B-PS, when a low potential is applied, the micelles may leave their position and the growth of the horns stops as shown in Figure 3a. When the applied potential is high enough to pull the micelles too intimate toward the substrate, the horns fade away as shown in Figure 3f.

In the case of PPy@A-PPS, the initial state and the first high potential period are similar to those of PPy@A-PS, the micelles are adsorbed tightly onto the substrate, and the polypyrrole grows over the micelles (Figure 11C1, C2). During the following low potential period of PPS, the micelles would be pushed away from the substrate because their electrical repulsion, as shown in Figure 11C3. When the applied φ_l and t_l are appropriately chosen, the micelles would be pushed further away but would not leave their position. In the following high potential period, the growth of polypyrrole along the micelle would start again, resulting in longer nanohorns with constant internal pore diameter, Figure 11C4. What is more, some more micelles would be probably adsorbed onto the substrate again at the beginning of each new period, and more equivalent nucleus and initial growth sites would be formed as a result of the desorption-adsorption processes. After several cycles of alternatively applying high and low potentials, uniform micro/nanostructured polypyrrole films would finally be obtained when proper potential parameters are applied, Figure 11C5. When the applied φ_l is too low, the micelles would leave their position during the low potential period and can hardly get back to their previous position during the following high potential period. As a consequence, very small and short micro/nanohorns would be obtained (Figure 4d).

In the case of PPy@B-PPS, the initial state and the first high potential period are similar to those of PPy@B-PS (Figure 11D1, D2). When the high potential is applied, the adhesion of the adsorbed micelles on the substrate is not so well, as shown in Figure 11D2. During the low potential periods, the adsorbed micelles could leave the substrate easier than that of PPy@A-PPS (Figure 11D3). If the low potential period is not long enough for the micelles to leave their initial place, things would happen similarly as PPy@A-PPS and the morphologies would be as shown in Figure 6a. Otherwise, in the following high potential periods, the short micro/nanohorns which are formed during the previous period would turn flat, and some new nucleus would form (Figure 11D4). Finally, the morphologies would be as shown in Figure 6d.

A conclusion can be tentatively drawn that the micelles which consist of pyrrole monomers and the surfactants work as the soft templates for the micro/nanohorn arrays. The electrochemical parameters, especially the low potential periods and OH^- in the solutions, influence the adsorption and desorption of the micelles and further affect the morphologies of PPy films. The balance of surfactants, pH value, potential type, and potential parameters results in the hollow micro/nanohorn arrays. Different from hard templates, the micelles "template" does not need to be removed after polymerization, because TOS^- plays the dopant role at the same time. It is a sort of template free method consequently.

Table 1. Selected FTIR and Raman Bands (cm^{-1}) of PPy@A-PS, PPy@B-PS, PPy@A-PPS, and PPy@B-PPS Films

FTIR (cm^{-1})					Raman (cm^{-1})			
PPy@A-PS	PPy@B-PS	PPy@A-PPS	PPy@B-PPS	assignments	PPy@A-PS	PPy@B-PS	PPy@A-PPS	PPy@B-PPS
2974	2987	2974	2971	$-CH_3$ asymmetric stretch vibration				
2943	2946	2945	2942	$-CH_2-$ asymmetric stretch vibration				
2874	2883	2877	2877	$-CH_3$ symmetric stretch vibration				
2790	2800	2790	2796	$-CH_2-$ symmetric stretch vibration				
				C═O stretch vibration	1764	1762	1764	1767
1580	1589	1577	1599	C═C stretch vibration of the pyrrole ring	1572	1575	1572	1574
1486	1489	1489	1495	C−N stretch vibration of the pyrrole ring	1488	1489	1488	1488
					1388	1385	1384	1384
1346	1342	1346	1349	antisymmetrical in-ring C−N stretch	1346	1345	1345	1345
1265	1263	1268	1263	antisymmetrical C−H in-plane bending	1255	1252	1255	1254
1228	1232	1224	1236	N−C stretch vibration				
1097	1093	1093	1099	=C−H in-plane vibration	1047	1048	1047	1047
1050	1060	1055	1057	N−H stretch vibration				
				benzoid formed ring vibration	977	977	976	975
				C−H out of the plane deformation	934	933	933	934
				C−H wagging	688	688	688	688
				ring torsion	622	622	622	622

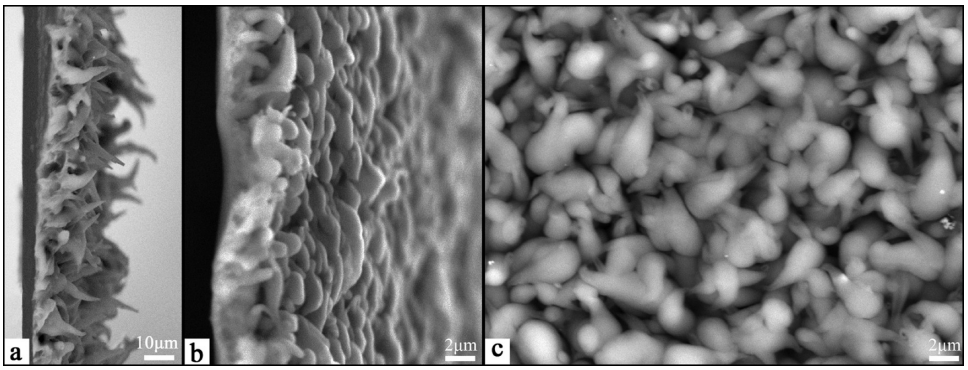

Figure 13. SEM images of the cross section of the unpressed PPy@A-PPS (a), pressed PPy@A-PPS (b), and the top view of the pressed PPy@A-PPS (c).

3. Structural Characterization and Electrical Conductivity. The resonance Raman spectra of PPy@A-PS, PPy@B-PS, PPy@A-PPS, and PPy@B-PPS films are presented in Figure 12a, which shows that all PPy films have the same characteristic peaks, clearly suggesting that the inherent property of PPy is not disturbed in all methods. Prominent bands (a)−(k) in Figure 12a are shown in Table 1.[24,38,39,28] The relative conjugation length, determined by the ratio between the intensity of the (j) (oxidization state sensitive) to (i) (skeletal band), is calculated to be 2.81, 3.29, 2.67, and 2.83 for PPy@A-PS, PPy@A-PPS, PPy@B-PS, and PPy@B-PPS, respectively. PPy@A-PPS shows the highest ratio of all, and PPy@B-PS shows the lowest value. The greater conjugation length implies the higher polarizability, which is in direct correspondence with the increase of the room temperature conductivity. The ratio of the PPy prepared in the acid solution is higher than those prepared in the basic solution, and PPS is preferred for the preparation of high activity PPy compared with PS.

The FTIR spectra of PPy@A-PS, PPy@B-PS, PPy@A-PPS, and PPy@B-PPS films are presented in Figure 12b and Table 1. The sharp peaks at 2974 cm^{-1}, 2874 cm^{-1}, 2947 cm^{-1}, and 2790 cm^{-1} of the films are assigned to $-CH_3$ asymmetric stretch vibration, $-CH_3$ symmetric stretch vibration, $-CH_2-$ asymmetric stretch vibration, and $-CH_2-$ symmetric stretch, respectively. PPy films prepared in acid solution show a weaker reflection band in the region 2830−2980 cm^{-1} than those prepared in basic solution, and PPy films prepared by a pulse potentiostatic method (PPS) show a weaker reflection band in the region 2830−2980 cm^{-1} than those prepared by a potentiostatic method (PS). The peaks of PPy@A-PPS are almost absent in this region. The reason of this was discussed in previous works.[20] The stretching band of C═O are observed at about 1765 cm^{-1} in all PPy films, which is due to overoxidation of carbon at the β positions of the pyrrole rings.[40] As $-CH_3$ and $-CH_2-$ are nonconducting polymer chains, the formation of these chains can decrease the electronic conductivity and electrochemical properties of PPy films prepared in basic solution or by a potentiostatic method. The reflection peaks below 2000 cm^{-1} are similar to the result of resonance Raman spectra.

A standard four-probe method is employed to get the conductivity of PPy films at the room temperature. The samples are prepared with the equivalent polymerization charge of 1500 mC to peel them off from the FTO glass. As shown in Figure 13a, PPy@A-PPS is so thin except for the part of micro/nanohorns that the film cannot connect well with the probes, leading to an incorrect result. To get closer to the real electronic conductivity, all PPy films are pressed under the pressure of 15 MPa before the test. The cross section and

surface of the pressed PPy@A-PPS is shown in Figure 13b and Figure 13c. We can see that the surface is flatter but still uneven, and the result may be smaller than the true value; so here the given values of PPy@A-PPS and PPy@B-PS are just for comparison. The measured σ_{RT} of PPy@A-PS, PPy@A-PPS, PPy@B-PS, and PPy@B-PPS is 90 S cm^{-1}, 190 S cm^{-1}, 40 S cm^{-1}, and 70 S cm^{-1}, respectively. Acid solutions and PPS are preferred to get PPy films with high conductivity.

CONCLUSIONS

In conclusion, a template-free electrochemical method is proposed to in situ synthesize PPy films with hollow micro/nanohorn arrays. A pulse potentiostatic method (PPS), especially the low potential periods, shows strong effect on the morphologies of PPy and is beneficial to improve the conductivity of PPy. 10^7−10^8 micro/nanohorns per square centimeter could be obtained almost vertically aligned on the substrate when PPS is applied in an acid aqueous solution of TOS^-. Based on comparison between different preparation conditions, a diagram is summarized, and the growth mechanism of the micro/nanohorn arrays is proposed. Briefly, the micelles which consist of pyrrole monomers and the surfactants work as the soft templates for the micro/nanohorns, and the electrochemical parameters influence the shape of the micelles at the substrate/electrolyte interface and further control the morphologies of PPy films. The developed method opens a facile way to in situ synthesize PPy micro/nanohorn arrays in aqueous solutions and has the potential to be developed as a general method for in situ synthesis of oriented micro/nanostructured conducting polymers.

ASSOCIATED CONTENT

Supporting Information

Explanation for the change of pH value with the polymerization process of PPy. Figures of PPy@A-PS and figures corresponding to Figure 10. This material is available free of charge via the Internet at http://pubs.acs.org.

AUTHOR INFORMATION

Corresponding Author

*Fax: +86 29 82665161. E-mail: ylxu@mail.xjtu.edu.cn.

Author Contributions

The manuscript was written through contributions of all authors. All authors have given approval to the final version of the manuscript.

Notes

The authors declare no competing financial interest.

ACKNOWLEDGMENTS

The authors are thankful for the financial support from the National Natural Science Foundation of China (Grant No. 21274115, 21203145, and 51201128), the program for new century excellent talents at the University of China (Grant No. NCET-11-0433), and the specialized research fund for the doctoral program of higher education of China (Grant No. 20110201130005). The authors also thank Ms. Lu Lu and Mr. Chuansheng Ma at the International Center for Dielectric Research for their help in using TEM.

ABBREVIATIONS

Py, pyrrole
PPy, polypyrrole
PS, potentiostatic
PPS, pulse potentiostatic
A, acid
B, basic

REFERENCES

(1) Tat'yana, V. V.; Oleg, N. E. Polypyrrole: A Conducting Polymer; Its Synthesis, Properties and Applications. *Russ. Chem. Rev.* **1997**, *66*, 443.
(2) Bredas, J. L.; Silbey, R.; Boudreaux, D. S.; Chance, R. R. Chain-Length Dependence of Electronic and Electrochemical Properties of Conjugated Systems: Polyacetylene, Polyphenylene, Polythiophene, and Polypyrrole. *J. Am. Chem. Soc.* **1983**, *105*, 6555−6559.
(3) Si, P.; Ding, S.; Lou, X.-W.; Kim, D.-H. An Electrochemically Formed Three-Dimensional Structure of Polypyrrole/Graphene Nanoplatelets for High-Performance Supercapacitors. *RSC Adv.* **2011**, *1*, 1271−1278.
(4) Chang, H. H.; Chang, C. K.; Tsai, Y. C.; Liao, C. S. Electrochemically Synthesized Graphene/Polypyrrole Composites and Their Use in Supercapacitor. *Carbon* **2012**, *50*, 2331−2336.
(5) Cui, Y. M.; Wen, Z. Y.; Liang, X.; Lu, Y.; Jin, J.; Wu, M. F.; Wu, X. W. A Tubular Polypyrrole Based Air Electrode with Improved O-2 Diffusivity for Li-O-2 Batteries. *Energy Environ. Sci.* **2012**, *5*, 7893−7897.
(6) Ravichandran, S.; Nagarajan, S.; Kokil, A.; Ponrathnam, T.; Bouldin, R. M.; Bruno, F. F.; Samuelson, L.; Kumar, J.; Nagarajan, R. Micellar Nanoreactors for Hematin Catalyzed Synthesis of Electrically Conducting Polypyrrole. *Langmuir* **2012**, *28*, 13380−13386.
(7) Gelmi, A.; Higgins, M. J.; Wallace, G. G. Resolving Sub-Molecular Binding and Electrical Switching Mechanisms of Single Proteins at Electroactive Conducting Polymers. *Small* **2013**, *9*, 393−401.
(8) Song, H. S.; Kwon, O. S.; Lee, S. H.; Park, S. J.; Kim, U. K.; Jang, J.; Park, T. H. Human Taste Receptor-Functionalized Field Effect Transistor as a Human-Like Nanobioelectronic Tongue. *Nano Lett.* **2013**, *13*, 172−178.
(9) Xue, M. Q.; Li, F. W.; Wang, Y.; Cai, X. J.; Pan, F.; Chen, J. T. Ultralow-Limit Gas Detection in Nano-Dumbbell Polymer Sensor Via Electrospinning. *Nanoscale* **2013**, *5*, 1803−1805.
(10) Ma, M. M.; Guo, L.; Anderson, D. G.; Langer, R. Bio-Inspired Polymer Composite Actuator and Generator Driven by Water Gradients. *Science* **2013**, *339*, 186−189.
(11) Zheng, W.; Razal, J. M.; Spinks, G. M.; Truong, V. T.; Whitten, P. G.; Wallace, G. G. The Role of Unbound Oligomers in the Nucleation and Growth of Electrodeposited Polypyrrole and Method for Preparing High Strength, High Conductivity Films. *Langmuir* **2012**, *28*, 10891−10897.
(12) Richard Prabakar, S. J.; Pyo, M. Corrosion Protection of Aluminum in Lipf6 by Poly(3,4-Ethylenedioxythiophene) Nanosphere-Coated Multiwalled Carbon Nanotube. *Corros. Sci.* **2012**, *57*, 42−48.
(13) Makris, T.; Dracopoulos, V.; Stergiopoulos, T.; Lianos, P. A Quasi Solid-State Dye-Sensitized Solar Cell Made of Polypyrrole Counter Electrodes. *Electrochim. Acta* **2011**, *56*, 2004−2008.
(14) Bu, C.; Tai, Q.; Liu, Y.; Guo, S.; Zhao, X. A Transparent and Stable Polypyrrole Counter Electrode for Dye-Sensitized Solar Cell. *J. Power Sources* **2013**, *221*, 78−83.
(15) Zhou, M.; Heinze, J. Electropolymerization of Pyrrole and Electrochemical Study of Polypyrrole: 1. Evidence for Structural Diversity of Polypyrrole. *Electrochim. Acta* **1999**, *44*, 1733−1748.
(16) Zhou, M.; Heinze, J. Electropolymerization of Pyrrole and Electrochemical Study of Polypyrrole. 2. Influence of Acidity on the Formation of Polypyrrole and the Multipathway Mechanism. *J. Phys. Chem. B* **1999**, *103*, 8443−8450.
(17) Song, J.; Liu, H.; Wan, M.; Zhu, Y.; Jiang, L. Bio-Inspired Isotropic and Anisotropic Wettability on a Janus Free-Standing Polypyrrole Film Fabricated by Interfacial Electro-Polymerization. *J. Mater. Chem. A* **2013**, *1*, 1740−1744.

(18) Santos, L.; Martin, P.; Ghilane, J.; Lacaze, P. C.; Lacroix, J.-C. Micro/Nano-Structured Polypyrrole Surfaces on Oxidizable Metals as Smart Electroswitchable Coatings. *ACS Appl. Mater. Interfaces* **2013**, *5*, 10159−10164.
(19) Tang, Y. H.; Wu, N.; Luo, S. L.; Liu, C. B.; Wang, K.; Chen, L. Y. One-Step Electrodeposition to Layer-by-Layer Graphene-Conducting-Polymer Hybrid Films. *Macromol. Rapid Commun.* **2012**, *33*, 1780−1786.
(20) Wang, J. P.; Xu, Y. L.; Wang, J.; Du, X. F.; Xiao, F.; Li, J. B. High Charge/Discharge Rate Polypyrrole Films Prepared by Pulse Current Polymerization. *Synth. Met.* **2010**, *160*, 1826−1831.
(21) Martin, C. R. Nanomaterials: A Membrane-Based Synthetic Approach. *Science* **1994**, *266*, 1961−1966.
(22) Zhang, J.; Liu, X. H.; Zhang, L. X.; Cao, B. Q.; Wu, S. H. Reactive Template Synthesis of Polypyrrole Nanotubes for Fabricating Metal/Conducting Polymer Nanocomposites. *Macromol. Rapid Commun.* **2013**, *34*, 528−532.
(23) Lee, J. I.; Cho, S. H.; Park, S.-M.; Kim, J. K.; Kim, J. K.; Yu, J.-W.; Kim, Y. C.; Russell, T. P. Highly Aligned Ultrahigh Density Arrays of Conducting Polymer Nanorods Using Block Copolymer Templates. *Nano Lett.* **2008**, *8*, 2315−2320.
(24) Duchet, J.; Legras, R.; Demoustier-Champagne, S. Chemical Synthesis of Polypyrrole: Structure−Properties Relationship. *Synth. Met.* **1998**, *98*, 113−122.
(25) Nam, D.-H.; Kim, M.-J.; Lim, S.-J.; Song, I.-S.; Kwon, H.-S. Single-Step Synthesis of Polypyrrole Nanowires by Cathodic Electropolymerization. *J. Mater. Chem. A* **2013**, *1*, 8061−8068.
(26) Wan, M. A Template-Free Method Towards Conducting Polymer Nanostructures. *Adv. Mater.* **2008**, *20*, 2926−2932.
(27) McCarthy, C. P.; McGuinness, N. B.; Alcock-Earley, B. E.; Breslin, C. B.; Rooney, A. D. Facile Template-Free Electrochemical Preparation of Poly N-(2-Cyanoethyl)Pyrrole Nanowires. *Electrochem. Commun.* **2012**, *20*, 79−82.
(28) Gupta, S. Template-Free Synthesis of Conducting-Polymer Polypyrrole Micro/Nanostructures Using Electrochemistry. *Appl. Phys. Lett.* **2006**, 88.
(29) Qu, L.; Shi, G.; Chen, F. e.; Zhang, J. Electrochemical Growth of Polypyrrole Microcontainers. *Macromolecules* **2003**, *36*, 1063−1067.
(30) Qu, L.; Shi, G. Electrochemical Synthesis of Novel Polypyrrole Microstructures. *Chem. Commun.* **2003**, *0*, 206−207.
(31) Massafera, M. P.; Córdoba de Torresi, S. I. Evaluating the Performance of Polypyrrole Nanowires on the Electrochemical Sensing of Ammonia in Solution. *J. Electroanal. Chem.* **2012**, *669*, 90−94.
(32) Debiemme-Chouvy, C. Template-Free One-Step Electrochemical Formation of Polypyrrole Nanowire Array. *Electrochem. Commun.* **2009**, *11*, 298−301.
(33) Wang, J.; Xu, Y.; Yan, F.; Zhu, J.; Wang, J. Template-Free Prepared Micro/Nanostructured Polypyrrole with Ultrafast Charging/Discharging Rate and Long Cycle Life. *J. Power Sources* **2011**, *196*, 2373−2379.
(34) Yang, Y.; Wan, M. Microtubules of Polypyrrole Synthesized by an Electrochemical Template-Free Method. *J. Mater. Chem.* **2001**, *11*, 2022−2027.
(35) Burda, C.; Chen, X.; Narayanan, R.; El-Sayed, M. A. Chemistry and Properties of Nanocrystals of Different Shapes. *Chem. Rev.* **2005**, *105*, 1025−1102.
(36) Liu, J.; Wan, M. Synthesis, Characterization and Electrical Properties of Microtubules of Polypyrrole Synthesized by a Template-Free Method. *J. Mater. Chem.* **2001**, *11*, 404−407.
(37) Jeon, S. S.; Kim, C.; Ko, J.; Im, S. S. Spherical Polypyrrole Nanoparticles as a Highly Efficient Counter Electrode for Dye-Sensitized Solar Cells. *J. Mater. Chem.* **2011**, *21*, 8146−8151.
(38) Montoya, P.; Jaramillo, F.; Calderón, J.; Córdoba de Torresi, S. I.; Torresi, R. M. Evidence of Redox Interactions between Polypyrrole and Fe_3O_4 in Polypyrrole−Fe_3O_4 Composite Films. *Electrochim. Acta* **2010**, *55*, 6116−6122.
(39) Santos, M. J. L.; Brolo, A. G.; Girotto, E. M. Study of Polaron and Bipolaron States in Polypyrrole by in Situ Raman Spectroelectrochemistry. *Electrochim. Acta* **2007**, *52*, 6141−6145.
(40) Ghosh, S.; Bowmaker, G. A.; Cooney, R. P.; Seakins, J. M. Infrared and Raman Spectroscopic Studies of the Electrochemical Oxidative Degradation of Polypyrrole. *Synth. Met.* **1998**, *95*, 63−67.